Exploring the possibilities of increasing energy density and efficiency in rechargeable batteries

Download this complimentary article collection

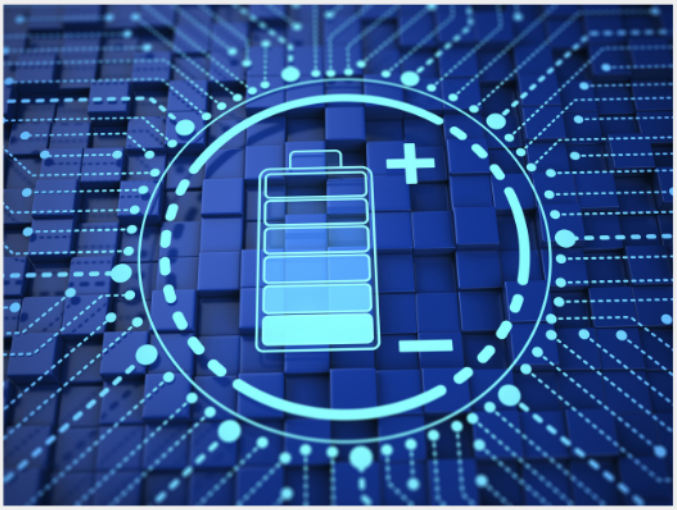

The exponential rise in the need for better, more efficient power sources has sparked an incredible amount of research into batteries. A primary focus of research has been increasing the energy density of batteries, as it allows for lighter, more portable storage of energy. Lithium-ion batteries, for example, have a much higher energy density than conventional lead-acid batteries and can be used for various purposes, such as in electric vehicles.

This article collection provides a comprehensive list of references for new methods and technologies for increasing the energy density of batteries.

Metrohm

WILEY

ADVANCED FUNCTIONAL MATERIALS
www.afm-journal.de

Thermosensitive Plasmonic Color Enabled by Sodium Metasurface

Yinghao Zhao, Yuhan Yang, Changyin Ji, Qinghua Liang, Hanyu Fu, Xing Liu, Lin Zhou, Jiafang Li,* and Yang Wang**

Active plasmonic nanostructures have attracted tremendous interest in nanophotonics and metamaterials owing to the dynamically switchable capabilities of plasmonic resonances. In this study, tunable hybrid plasmon resonances (HPR) of sodium metasurfaces through heat-initiated structural transformation is experimentally demonstrated. A HPR is formed by coupling surface plasmon polaritons (SPP) and gap plasmon resonances (GPR), whose resonant wavelengths are highly sensitive to gaseous nanogaps. By carefully manipulating the thermo-assisted spin-coating process and post-thermal treatment, tuning of the HPR is achieved because of the phase transition between the antidome and nanodome structural profiles of liquid sodium inside the patterned fused silica substrates. Furthermore, the figure of merit of the heat initiated variable structure-spectrum is demonstrated that is highly dependent on the size of the substrate patterns, based on which temperature-sensitive plasmonic color and "invisible ink" of sodium metasurfaces are demonstrated. These findings can lead to new solutions for manipulating low-cost and high-performance active plasmonic devices.

1. Introduction

Plasmonics has attracted extensive research interest for its strong enhancement of linear and nonlinear optical process at nanoscale, and has promoted the emergence and development of many nanophotonic phenomena and devices, such as super-resolution imaging,[1] plasmonic waveguides/circuits,[2,3] nanolasers,[4,5] surface-enhanced Raman scattering,[6] plasmonic holography,[7,8] plasmonic enhanced photovoltaics,[9] etc. With the development of nanotechnology over the past two decades, researchers have successfully prepared various plasmonic micro- and nanostructures and metasurfaces. Particularly, metasurfaces provide a route for efficient planar photonics with different functions integrated into a single device, such as optical information multiplexing,[10] 3D positioning,[11] and multifunctional spin-selective design.[12] Among the many plasmonic materials, sodium—an alkali metal—has attracted much attention because of its low intraband optical loss and electron gas density compared to those of noble metals.[13-15] Using thermo-assisted spin-coating technique, the performance of sodium-based devices can be enhanced to twice that of silver with long-term stability at near-infrared wavelengths.[16] Moreover, sodium is more abundant than noble metals on Earth, with well-established industrial fabrication processes; therefore, it is an ideal candidate for large-scale industrial implementation of nanophotonic devices.

The intriguing plasmonic properties of sodium has inspired considerable research on the dynamic plasmonic strategies with alkali metals for adaptation to modern optical systems and practical applications such as displays,[17] tunable beam shaping, and spatial light modulators.[18] Known as a unique plasmonic materials beyond noble metals, alkali metals are characterized by extremely high chemical activity, which has long hindered the development of applicable devices. However, it does open new doors for the dynamic plasmonics except for conventional strategies such as refractive index/polarization manipulation enabled by liquid crystal or polarizer,[19–23] oxidation and reduction of metals and semiconductors,[24,25] electrochemical deposition,[26,27] electrochromic polymers,[28,9] assembly/disassembly of silver nanoparticles,[30,31] and thermosensitive phase change materials,[32–35] etc. In the past few years, the electrochemical processing of lithium has been successfully introduced for switchable plasmonic and operando plasmonic monitoring.[36,37] Recently, this technique has been employed in low-power dynamic displays with long-term cycling performance.[38] Furthermore, the thermo-assisted spin-coating

Y. Zhao, C. Ji, Q. Liang, X. Liu, J. Li, Y. Wang
Key Lab of Advanced Optoelectronic Quantum Architecture and Measurement (Ministry of Education)
Beijing Key Lab of Nanophotonics & Ultrafine Optoelectronic Systems and School of Physics
Beijing Institute of Technology
Beijing 100081, China
E-mail: jiafangli@bit.edu.cn; yangwang@bit.edu.cn
Y. Yang, H. Fu, L. Zhou
National Laboratory of Solid State Microstructures
College of Engineering and Applied Sciences
School of Physics
Key Laboratory of Intelligent Optical Sensing and Integration and Collaborative Innovation Center of Advanced Microstructures
Nanjing University
Nanjing 210093, China
E-mail: linzhou@nju.edu.cn

The ORCID identification number(s) for the author(s) of this article can be found under https://doi.org/10.1002/adfm.202214492

DOI: 10.1002/adfm.202214492

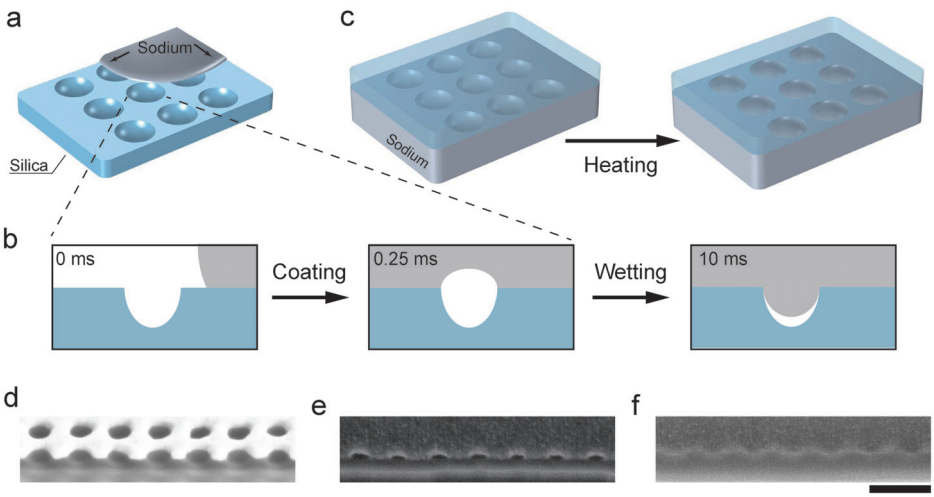

Figure 1. Heat-initiated structural transformation of sodium metasurface. a) Schematic of the formation of sodium metasurface. b) Simulation of the wetting process of liquid sodium on silica nanopore (details in Note S1, Supporting Information). c) Schematic of structural transformation of sodium metasurface, from anti-domes to nanodomes. d) SEM image of the silica template, with periodic nanopores. e) SEM image of the interface of sodium and silica before transformation. f) SEM image of the interface after transformation. Scale bar for d), e), and f): 500 nm.

technique was used to prepare sodium nanostructures, making thermal control an alternative unique strategy for fine-tuning the plasmonic properties of sodium because of its relatively low melting point. Liquid metals are potentially dynamic materials because of their deformable and movable properties, and the manipulation of liquid metals on the centimeter scale has been demonstrated using electrowetting and chemical methods.[39,40] Unfortunately, the precise thermo-assisted optical control of sodium metals remains challenging because of the difficulty in the thermal management of microstructures.

In this study, we developed a thermo-assisted spin-coating technique and demonstrated a method for manipulating sodium metasurfaces based on direct heating. By rapidly cooling liquid sodium onto silica nanopores, periodic sodium anti-dome structures with gaseous nanogaps, which can shrink after the sodium melts, were realized. Based on this new technique, tunable reflection of the sodium plasmonic structure was demonstrated by utilizing the wetting process at the interface of liquid sodium and silica. Temperature warning and information cloaking functions were achieved through this irreversible spectral change process. This sodium-based plasmonic color-manipulation strategy may provide an alternative route for sensors, information encryption, displays, and holography.

2. Results and Discussion

The key to achieving the modulation capability of plasmonic structures is to rapidly cool the liquid-phase sodium on silica nanopores. **Figure 1**a illustrates the formation of a sodium-based plasmonic metasurface using the proposed rapid-cooling-assisted spin-coating technique. A focused ion beam (FIB) was used to mill nanohole patterns with various periods and diameters on a silica substrate. Subsequently, molten sodium was spin-coated onto it. In addition to being the template, the silica substrate acted as a protective layer to prevent sodium oxidation. During the spin-coating of liquid sodium, there was a nonwetting period. To explore the formation mechanism of sodium nanostructures, we simulated the wetting process of liquid sodium (Figure 1b, see details in Note S1, Supporting Information), which demonstrated that the nanopores reduced the interface wettability compared with a smooth interface. When flowing through the silica nanopores, liquid sodium initially forms an anti-dome structure with a nanogap and gradually fills the pores over time. This process is very rapid, and anti-dome structure only appears in the first 0.25 ms. Generally, it is difficult to observe this intermediate state because the liquid metal continues to flow during the wetting processes. Herein, the structure of sodium was maintained in the anti-dome profile via the rapid cooling technique.

In contrast to previous spin coating method,[16] the operation temperature of sodium was kept at a lower value (≈140 °C). A lower temperature causes liquid sodium to cool more quickly allowing to shape the nanogaps before the sodium completely wets the silica nanopores. The existence of these sodium antidomes and gaseous nanogaps enable the regulation of the nanostructure by further heating. As shown in Figure 1c, when the sodium melted again, the wetting process continued, as described in the simulation, filling the pores and forming the nanodomes. Figure 1d–f shows the cross-sectional scanning electron microscopy (SEM) images of the prepared silica template and unfilled and filled sodium metasurfaces before and after heat treatment, respectively. Gaseous nanogaps and sodium anti-dome structures before heating and the sodium nanodome after structural transformation are evident.

Schematic morphologies of the sodium and gas nanogaps before and after heating are shown in the left and right panels of **Figure 2**a, respectively. Multipole decomposition calculations were performed using finite element method for the sodium nanostructure arrays (Note S2, Supporting Information). Figure 2b shows the reflection spectra before and after the structural transformation. The black line in Figure 2b indicates two resonant modes in the target wavelength range. The resonance wavelength of the first resonant mode is at $\lambda = 529$ nm, which is

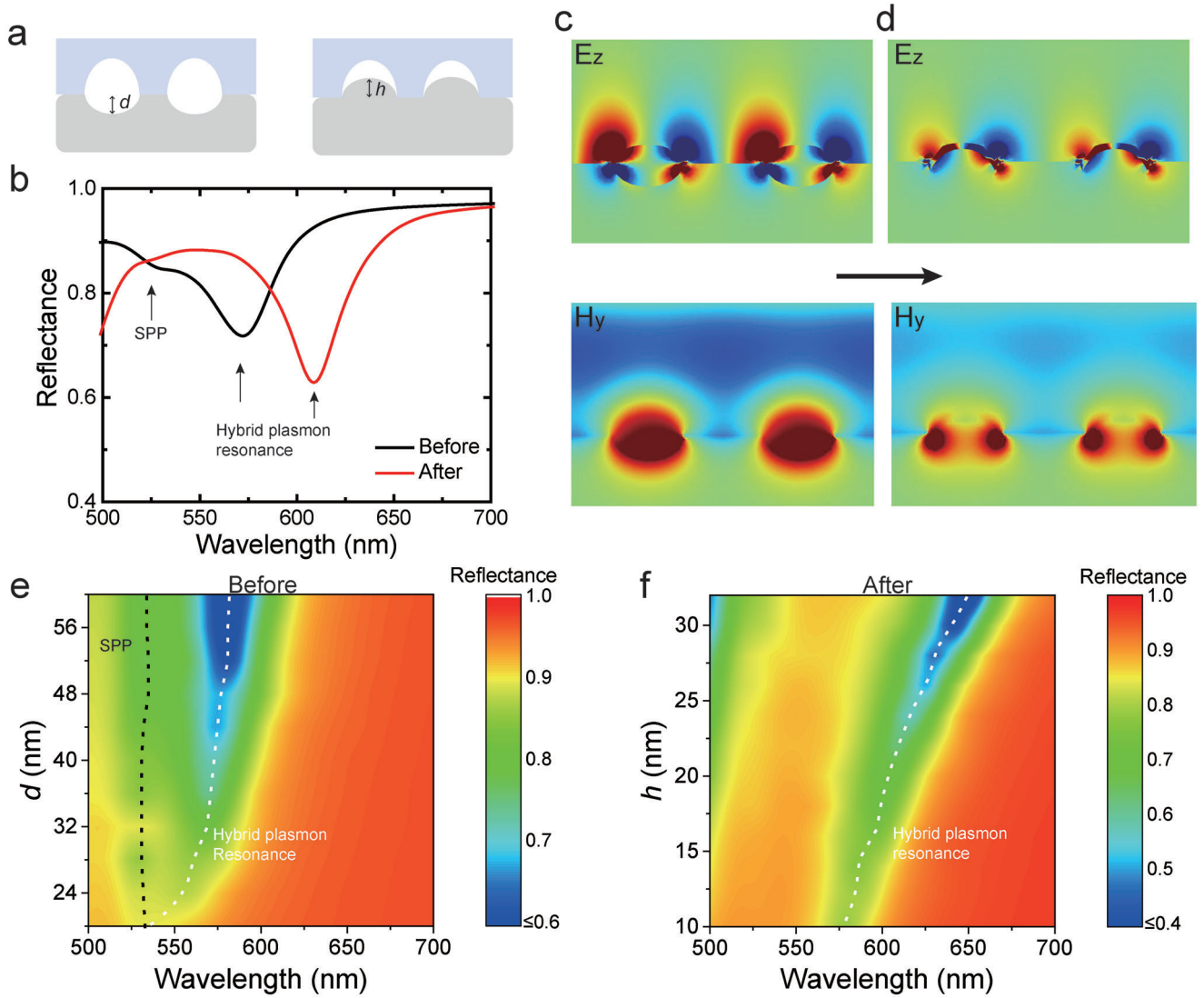

Figure 2. Simulation of sodium nanostructures before and after structural transformation. a) Schematic of structural transformation, from sodium anti-dome to nanodomes. The parameter *d* denotes the depth of anti-dome, and *h* denotes the height of nanodome. b) Reflection spectra of sodium nanostructures before and after transformation. We can see a red shift of the absorption valley. c) and d) Electric field E_z and magnetic field H_y distributions of the sodium anti-domes and nanodomes. e) Reflection spectra of sodium anti-domes as a function of the depth. f) Reflection spectra of sodium nanodomes as a function of the height.

induced by the surface plasmon polariton (SPP). The resonance wavelength of the second resonant mode is $\lambda = 575$ nm, which shifted to $\lambda = 625$ nm after heating (red line in Figure 2b). To reveal the physical origin of the large wavelength shift of the second resonant mode, electromagnetic-field distribution profiles before and after heating were evaluated, as shown in Figure 2c,d, respectively. The results in Figure 2c show that the electric field was concentrated at the sodium-gas and sodium-silica interfaces. The concentration of the electric field at the sodium-gas interface indicates that this mode resembles gap plasmon resonance (GPR), whereas that at the sodium-silica interface indicates that this mode resembles SPP. Thus, the second resonant mode can be considered as a hybrid of SPP and GPR, namely, hybrid plasmon resonance (HPR). After deformation, the electric field distributions of SPP and GPR became closer (Figure 2d). In such cases, the interaction between them is stronger than before heating, which significantly changes the resonant wavelength. Moreover, a magnetic hotspot was created using the HPR (lower panel of Figure 2d).

This spectral redshift from the antidome to dome is applicable to various nanogap parameters. We further plotted the reflection spectra of the sodium nanostructures as a function of the depth (*d*) and height (*h*) of the anti-dome/dome structure (Figure 2e and f). In Figure 2e, only one SPP mode is observed for the anti-dome with $d = 20$ nm. HPR appeared when *d* exceeded ≈20 nm, and its excitation became stronger and split from SPP as *d* increased. The degree of mode splitting reaches a maximum at a wavelength of ≈580 nm when $d = 56$ nm. For the dome structures shown in Figure 2f, the GPR and SPP distributions are much closer than those of the anti-dome structures, resulting in strong coupling. In

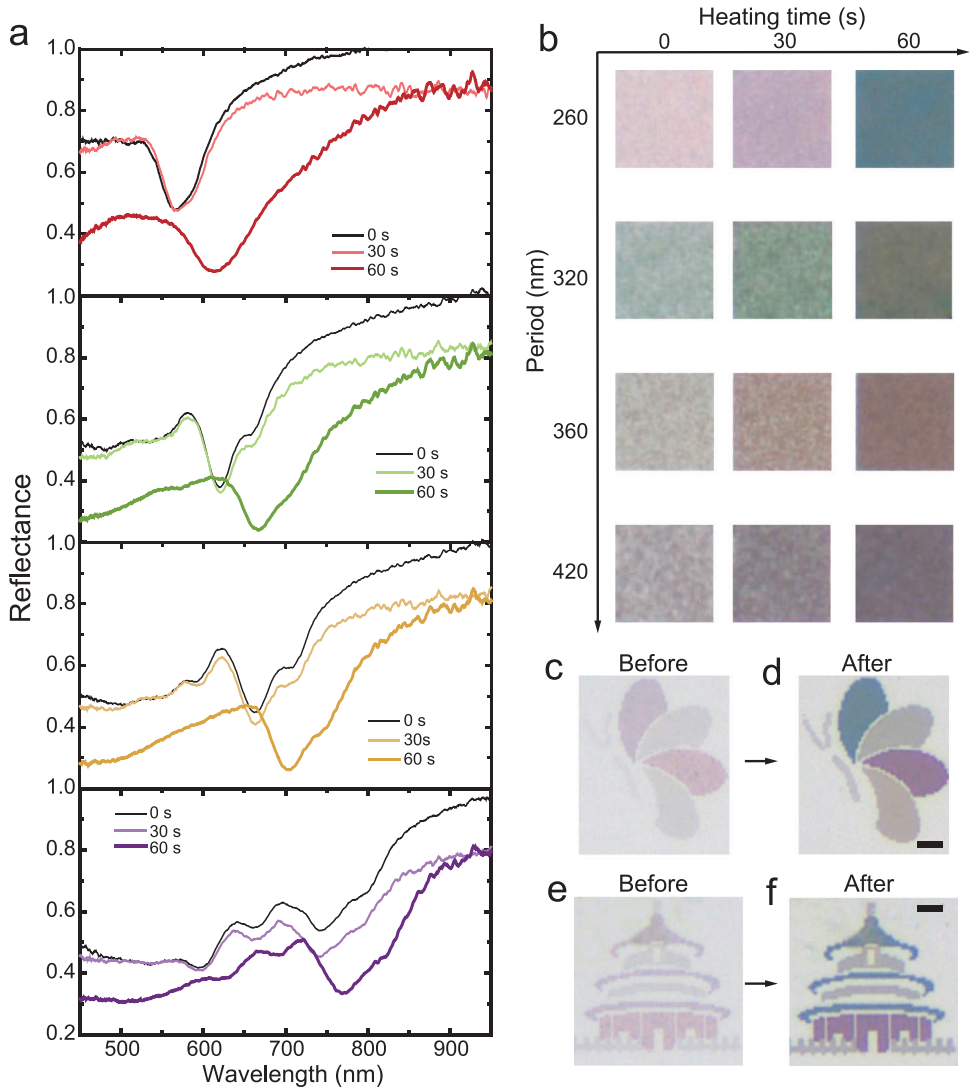

Figure 3. Experimental modulation of reflection spectrum and plasmonic colors of sodium. a) Experimental reflection spectra of the four structures at various heating time, with periods of 260, 320, 360, and 420 nm. b) Optical images of sodium nanostructure array under a 10× objective at various heating time. Each individual image area is 30×30 μm^2. c) and d) A butterfly painting based on sodium plasmonic colors before and after heating. e) and f) A temple painting based on sodium plasmonic colors before and after heating. Scale bar for c–f: 10 μm.

this case, the resonance wavelength of the HPR mode increases as h increases, reaching ≈650 nm when h = 32 nm. Moreover, the resonance absorption of the HPR became stronger. Thus, the redshift of the resonance wavelength of the HPR with different gap parameters before and after the structural transformation was more evident. The sensitivity of the resonant wavelength of the hybrid mode to the gas nanogap is expected to provide an advanced platform for plasmonic color modulation.

Plasmonic structural colors.[41–45] have important applications in imaging, displays, high-resolution printing, and optical data storage. Based on this technology, we further investigated sodium-based plasmonic colors. **Figure 3**a and b show the variation in the reflection spectra and optical images of the sodium nanostructures with different periods before and after heating for 30 and 60 s, respectively (for spectra with longer time, see Figure S4, Supporting Information). The temperature of heater was set to 120 °C. As the heating time increased, the reflection color changed owing to shifts in the resonance wavelengths caused by the structural transformation. The reflection spectrum changed slightly at the beginning, followed by a sudden large shift. The first stage can be explained by the simulation results shown in Figure 2e, in which the resonance wavelength did not change significantly as the depth of the anti-dome decreased. As the wetting process progressed, sodium began to fill the silica pores, resulting in a complete change in the structure and a dramatic shift in the spectrum, as shown by both the simulation (Figure 2b) and experimental (Figure 3a) results. Various plasmonic paintings can be created based on the structural colors of sodium. For the purpose of demonstration, butterfly and temple symbols for the different colored structures are shown in Figure 3c–f, with pixel units of 1×1 μm^2. The colors of the paintings were observed to change upon heating.

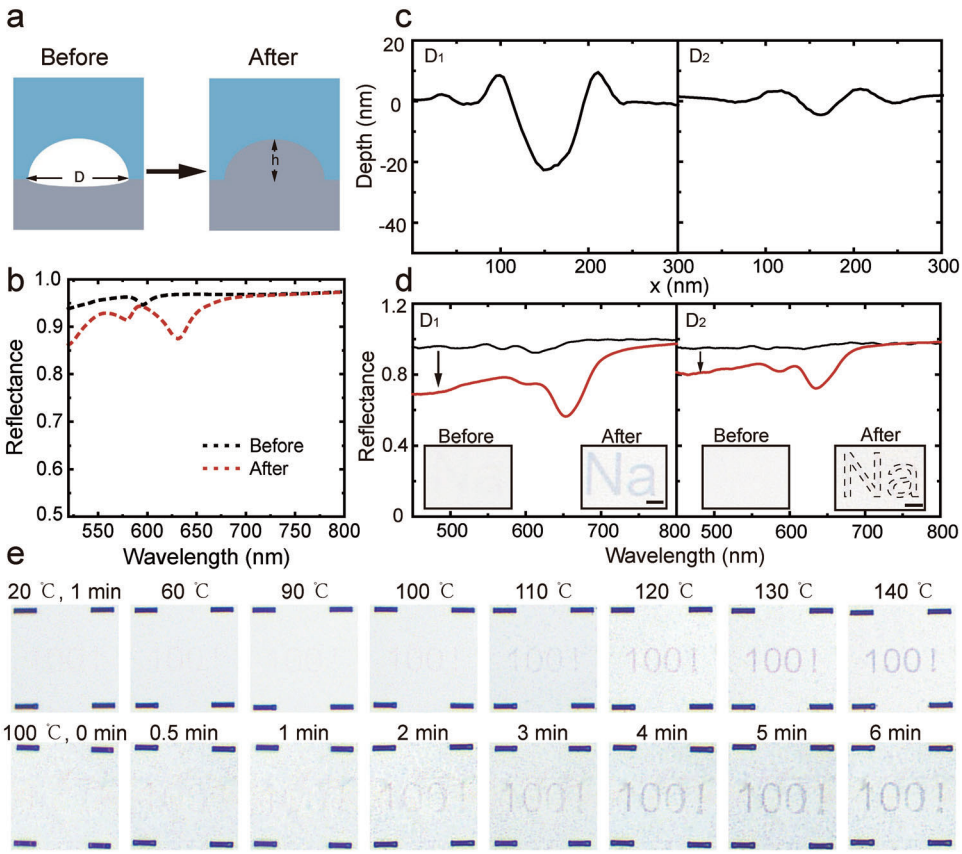

Figure 4. Information cloaking and temperature warning based on structural transformation of sodium metasurface. a) Schematic of structural transformation, from almost flat structure to nanodome. Gray represents sodium, blue represents silica. b) Reflection spectra of sodium nanostructures before and after transformation. c) The cross-section morphology of two silica templates with different pore sizes. The data is collected by atomic force microscope. $D_1 = 85$ nm, $D_2 = 50$ nm. d) Experimental reflection spectra of the sodium nanostructures before and after heating. Inset: optical images of the invisible letter painting before and after heating, the dotted line outlines the letter with smaller pore size. e) Optical images of the temperature warning painting (100!) with different temperatures (upper) and times (bottom). The length of the marks at corners is 10 μm.

Note that the initial color of the sample was lighter than that after the heat treatment, which was mainly due to the weaker resonance of the anti-dome structures. As shown in Figure 2b and c, the electric field distributions of the SPP and GPR modes of the anti-dome structure were more discrete than those of the dome structure, which weakened the hybrid resonance. Therefore, a shallower absorption valley was observed before heating, which results in a lower contrast. By further developing this feature, the function of "invisible ink" can be realized via precise control of the size of nanopore template.

The key point of the invisible design is to control the silica pore size to be sufficiently small to avoid a large curvature of the anti-dome structure during the spin-coating process, so that an approximate plane interface can be formed (**Figure 4**a). The simulation results show that the reflection spectrum approaches mirror reflection. However, after the structural transformation, the sodium metasurface exhibited a significant spectral valley, which caused the pattern to appear (Figure 4b). Figure 4c shows the cross-sectional morphology of the silica nanopores with diameters of 85 and 50 nm. Square regions with side lengths of 20 μm were prepared for spectral characterization (Figure 4d). For large nanopores with diameters >100 nm, a sodium antidome was formed after rapid-cooling spin coating, and optical responses of various colors appeared, as shown in Figure 3. However, the spin-coated sodium did not form obvious curves for small nanopores with diameters below 100 nm. The interface was close to a mirror surface that exhibited ≈100% reflection, leading to an invisible appearance. After heating, liquid sodium begins to fill the nanopores, forming periodic nanodomes, resulting in an absorption valley and forming the structure.

Based on the above experimental phenomena, we prepared invisible letter patterns "Na" with two sizes of nanopores template (Figure 4d, inset). The reflection spectra showed a very shallow absorption valley in the initial state for the pattern with the pore diameter of 85 nm, which was absent for the pattern with the pore diameter of 50 nm. Moreover, observing obvious colored regions in both patterns using an optical microscope was difficult. However, after heating, the pattern with a larger pore size exhibited a better color effect than that with a smaller pore size, mainly because of the deeper absorption valley after heating. As a result, the hidden letter "Na" was clearly revealed for structure with large pore size but remained almost invisible for structure with small pore size. This design clearly demonstrates the ability to encode and decode information by simple heating of the device.

Since the melting point of sodium is close to 100 °C, sodium devices are particularly suitable for temperature warning applications such as chips, steam, etc. We further characterized the dynamic response of the devices at different temperatures and heating times, shown in Figure 4e, with an invisible pattern of "100!". For the devices heated with different temperatures for 1 min, the pattern gradually became visible only when the temperature exceeds 100 °C. Furthermore, the changing process of sample under 100 °C were observed as a function of time. In the current packaging form, the device displays the pattern after 1 min. These data demonstrate the capability of the sodium metasurface for temperature warnings and sensing.

Therefore, compared with other dynamic plasmonic color methods (such as polarization control enabled by liquid crystals, chemical or electrochemical methods, etc.), the proposed manipulation strategy has a simple material structure and convenient tuning method that is environmentally responsive and does not rely on additional control devices, such as polarizers, liquid crystals, batteries, and chemicals. The structural unit of a sodium metasurface can be further designed in a polarized manner to form devices with multidimensional responses. More importantly, its response temperature and mirror/color-switching characteristics are significantly different from those of other dynamic plasmonic materials, enabling unique functions such as temperature warnings and information cloaking.

3. Conclusions

To summarize, we experimentally demonstrated a method for manipulating sodium-based plasmonic metasurfaces via heat-initiated structural transformation. Using a rapid-cooling spin-coating technique, plasmonic colors with sodium antidomes with gaseous nanogaps were realized. When sodium was heated to the liquid state again, a nanofluid transformation occurred near the silica nanopores, which changed the reflection spectrum and plasmonic color. Numerical analysis of sodium nanostructures proved that the color changes mainly originate from changes in the nanogap geometry, leading to shifts in the hybrid plasmon resonances. Finally, we designed and demonstrated a thermosensitive "invisible ink" device. These results show that sodium-based plasmonic metasurfaces have great potential for applications in passive sensors, information cloaking, optical data storage, imaging, and displays, providing alternative routes for the dynamic control of low-loss plasmonic devices.

4. Experimental Section

Fabrication of Sodium Metasurfaces: First, a piece of fresh sodium was cut with a knife in a glove box equipped with an inert atmosphere. The sodium was then melted on a heater with temperature of 140 °C to form a droplet. The oxide shell on the surface of the sodium droplets was peeled off using tweezers. The liquid sodium was then removed from the heater for a few seconds before being dropped onto a fast-spinning silica substrate, which was nanostructured by focused ion beam (FIB) milling. A thin silver film (thickness of ≈60 nm) was evaporated onto silica to form a conductive layer for scanning electron microscope imaging, and the nanohole arrays were patterned via FIB. The silver film was then removed using an HNO_3 solution.

Optical Measurements of the Sodium Metasurfaces: The sodium metasurface was covered with another silica substrate from the back and sealed it with epoxy to prevent air exposure before testing. The optical images and reflection spectra were obtained using a brightfield reflection microscope (Olympus BX) illuminated by a halogen light source (Ideaoptics HL2000, halogen light source) with a 10× (NA 0.3) objective. The reflection spectra were measured using a microspectrometer (Ideaoptics PG2000-Pro).

Supporting Information

Supporting Information is available from the Wiley Online Library or from the author.

Acknowledgements

Y.Z. and Y.Y. contributed equally to this work. This work was jointly supported by the National Natural Science foundation of China (grant nos. 62205022, 61975016, 12022403, 61735008), National Key Research and Development Program of China (nos. 2022YFA1404300, 2021YFA1400700), Natural Science Foundation of Beijing Municipality (grant nos. Z190006 and 1212013), Beijing Institute of Technology Research Fund Program for Young Scholars. The authors thank Analysis &Testing Center of Beijing Institute of Technology.

Conflict of Interest

The authors declare no conflict of interest.

Data Availability Statement

The data that support the findings of this study are available from the corresponding author upon reasonable request.

Keywords

information cloaking, plasmonic colors, sodium metasurfaces, temperature sensitive

Received: December 12, 2022
Revised: April 25, 2023
Published online:

[1] N. Fang, H. Lee, C. Sun, X. Zhang, *Science* **2005**, *308*, 534.
[2] R. F. Oulton, V. J. Sorger, D. A. Genov, D. F. P. Pile, X. Zhang, *Nat. Photonics* **2008**, *2*, 496.
[3] Y. Fu, X. Hu, C. Lu, S. Yue, H. Yang, Q. Gong, *Nano Lett.* **2012**, *12*, 5784.
[4] Y. J. Lu, J. Kim, H. Y. Chen, C. Wu, N. Dabidian, C. E. Sanders, C. Y. Wang, M. Y. Lu, B. H. Li, X. Qiu, W. H. Chang, L. J. Chen, G. Shvets, C. K. Shih, S. Gwo, *Science* **2012**, *337*, 450.
[5] R. M. Ma, R. F. Oulton, *Nat. Nanotechnol.* **2019**, *14*, 12.
[6] S. Jiang, Y. Zhang, R. Zhang, C. Hu, M. Liao, Y. Luo, J. Yang, Z. Dong, J. G. Hou, *Nat. Nanotechnol.* **2015**, *10*, 865.
[7] L. Huang, X. Chen, H. Mühlenbernd, H. Zhang, S. Chen, B. Bai, Q. Tan, G. Jin, K.-W. Cheah, C.-W. Qiu, J. Li, T. Zentgraf, S. Zhang, *Nat. Commun.* **2013**, *4*, 2808.
[8] J. Chen, T. Li, S. Wang, S. Zhu, *Nano Lett.* **2017**, *17*, 5051.
[9] H. A. Atwater, A. Polman, *Nat. Mater.* **2010**, *9*, 205.
[10] X. Ouyang, Y. Xu, M. Xian, X. Li, *Nat. Photonics* **2021**, *15*, 901.
[11] W. Liu, D. Ma, Z. Li, H. Cheng, S. Chen, *Optica.* **2020**, *7*, 1706.

[12] W. Liu, Z. Li, Z. Li, H. Cheng, C. Tang, J. Li, S. Chen, J. Tian, *Adv. Mater.* **2019**, *31*, 1901729.
[13] E. D. Palik, *Handbook of Optical Constants of Solids*, Academic Press, Cambridge, US **1998**.
[14] A. Boltasseva, H. A. Atwater, *Science* **2011**, *331*, 290.
[15] G. V. Naik, V. M. Shalaev, A. Boltasseva, *Adv. Mater.* **2013**, *25*, 3264.
[16] Y. Wang, J. Yu, Y. F. Mao, J. Chen, S. Wang, H. Z. Chen, Y. Zhang, S. Y. Wang, X. Chen, T. Li, L. Zhou, R. M. Ma, S. Zhu, W. Cai, J. Zhu, *Nature* **2020**, *581*, 401.
[17] F. Neubrech, X. Duan, N. Liu, *Sci. Adv.* **2020**, *6*, eabc2709.
[18] A. L. Holsteen, A. F. Cihan, M. L. Brongersma, *Science* **2019**, *365*, 257.
[19] D. Franklin, Y. Chen, A. Vazquez-Guardado, S. Modak, J. Boroumand, D. Xu, S. T. Wu, D. Chanda, *Nat. Commun.* **2015**, *6*, 7337.
[20] D. Franklin, R. Frank, S. T. Wu, D. Chanda, *Nat. Commun.* **2017**, *8*, 15209.
[21] V. R. Shrestha, S. S. Lee, E. S. Kim, D. Y. Choi, *Sci. Rep.* **2015**, *5*, 12450.
[22] I. Koirala, V. R. Shrestha, C. S. Park, S. S. Lee, D. Y. Choi, *Sci. Rep.* **2017**, *7*, 40073.
[23] E. Balaur, C. Sadatnajafi, S. S. Kou, J. Lin, B. Abbey, *Sci. Rep.* **2016**, *6*, 28062.
[24] X. Duan, S. Kamin, N. Liu, *Nat. Commun.* **2017**, *8*, 14606.
[25] Y. Nagasaki, M. Suzuki, I. Hotta, J. Takahara, *ACS Photonics* **2018**, *5*, 1460.
[26] Z. Yan, Z. Zhang, W. Wu, X. Ji, S. Sun, Y. Jiang, C. C. Tan, L. Yang, C. T. Chong, C. W. Qiu, R. Zhao, *Nat. Nanotechnol.* **2021**, *16*, 795.
[27] A. Tsuboi, K. Nakamura, N. Kobayashi, *Adv. Mater.* **2013**, *25*, 3197.
[28] K. Xiong, G. Emilsson, A. Maziz, X. Yang, L. Shao, E. W. Jager, A. B. Dahlin, *Adv. Mater.* **2016**, *28*, 9956.
[29] P. A. Ledin, J. W. Jeon, J. A. Geldmeier, J. F. Ponder Jr., M. A. Mahmoud, M. El-Sayed, J. R. Reynolds, V. V. Tsukruk, *ACS Appl. Mater. Interfaces* **2016**, *8*, 13064.
[30] A. Tsuboi, K. Nakamura, N. Kobayashi, *Adv. Mater.* **2013**, *25*, 3197.
[31] S. Araki, K. Nakamura, K. Kobayashi, *Adv. Mater.* **2012**, *24*, OP122.
[32] F. Z. Shu, F. F. Yu, R. W. Peng, Y. Y. Zhu, B. Xiong, R. H. Fan, Z. H. Wang, Y. Liu, M. Wang, *Adv. Opt. Mater.* **2018**, *6*, 1700939.
[33] T. Cao, X. Zhang, W. Dong, L. Lu, X. Zhou, X. Zhuang, J. Deng, X. Cheng, G. Li, R. E. Simpson, *Adv. Opt. Mater.* **2018**, *6*, 1800169.
[34] X. Liu, Q. Wang, X. Zhang, H. Li, Q. Xu, Y. Xu, X. Chen, S. Li, M. Liu, Z. Tian, C. Zhang, C. Zou, J. Han, W. Zhang, *Adv. Opt. Mater.* **2019**, *7*, 1900175.
[35] F. Z. Shu, J. N. Wang, R. W. Peng, B. Xiong, R. H. Fan, Y. J. Gao, Y. Liu, D. X. Qi, M. Wang, *Laser Photonics Rev.* **2021**, *15*, 2100155.
[36] Y. Jin, L. Zhou, J. Yu, J. Liang, W. Cai, H. Zhang, S. Zhu, J. Zhu, *Proc. Natl. Acad. Sci. USA* **2018**, *115*, 11168.
[37] Y. Jin, J. Liang, S. Wu, Y. Zhang, L. Zhou, Q. Wang, H. Liu, J. Zhu, *Adv. Mater.* **2020**, *32*, 2000058.
[38] J. Liang, Y. Jin, H. Yu, X. Chen, L. Zhou, P. Huo, Y. Zhang, H. Ma, Y. Jiang, B. Zhu, T. Xu, H. Liu, S. Zhu, J. Zhu, *Natl. Sci. Rev.* **2022**, *10*, nwac120.
[39] L. Sheng, J. Zhang, J. Liu, *Adv. Mater.* **2014**, *26*, 6036.
[40] J. Zhang, Y. Yao, L. Sheng, J. Liu, *Adv. Mater.* **2015**, *27*, 2648.
[41] K. Kumar, H. Duan, R. S. Hegde, S. C. Koh, J. N. Wei, J. K. Yang, *Nat. Nanotechnol.* **2012**, *7*, 557.
[42] T. Xu, Y. K. Wu, X. Luo, L. J. Guo, *Nat. Commun.* **2010**, *1*, 59.
[43] Z. Li, A. W. Clark, J. M. Cooper, *ACS Nano* **2016**, *10*, 492.
[44] H. Wang, X. Wang, C. Yan, H. Zhao, J. Zhang, C. Santschi, O. J. F. Martin, *ACS Nano* **2017**, *11*, 4419.
[45] X. Zhu, W. Yan, U. Levy, N. A. Mortensen, A. Kristensen, *Sci. Adv.* **2017**, *3*, e1602487.